SUPPORTING INFORMATION

Chinese Journal of Structural Chemistry

Ni_3N Modified MOF Heterostructure with Tailored Electronic Structure for Efficient Overall Water Splitting

Hongnan Jia[1†], Na Yao[1†], Juan Zhu[1], Yujia Liu[1], Yunhao Lao[1], Hengjiang Cong[1*] and Wei Luo[1,2*]

[1]*College of Chemistry and Molecular Sciences, Wuhan University, Wuhan 430072, China*
[2]*Suzhou Institute of Wuhan University, Suzhou, Jiangsu 215123, China*

**Corresponding authors. E-mails: conghj@whu.edu.cn and wluo@whu.edu.cn*

SUPPORTING INFORMATION

Chinese Journal of Structural Chemistry

n EXPERIMENT

Materials. Nickel (II) nitrate hexahydrate ($Ni(NO_3)_2·6H_2O$), N,N-dimethylformamide (DMF) and ethanol (EtOH) were purchased from China National Medicines Corporation Ltd.; 2,5-Dihydroxyterephthalic acid (H_2DOT) was purchased from Shanghai Macklin Biochemical Co., Ltd.; All chemicals were used without further purifications.

Synthesis of Ni-MOF-74 Precursor. $Ni(NO_3)_2·6H_2O$ (180 mg) and H_2BDC (38 mg) were completely dissolved in 3 mL of DMF by using the ultrasonic treatment in a 20 mL Pyrex vial. Deionized water (3 mL) and EtOH (3 mL) were added to the solution. The mixture was heated in an isothermal oven at 120 °C and allowed to react for 24 h to yield brown powder after cooling to room temperature. Then, the as-synthesized sample was subsequently treated with solvent exchange with DMF for 6 times and EtOH for 3 times. Later, the remaining EtOH in the MOF samples was removed under vacuum conditions.

Synthesis of Ni-MOF-74/Ni_3N. The as-prepared Ni-C precursor was put into a quartz boat and placed in the center of a tube furnace. The furnace was purged with mixture of gases (90% Ar and 10% H_2) overnight and then purged with ammonia for 60 minutes. Next, the furnace was heated to 350 °C and keep for 1 hours. After heating, the furnace was allowed to naturally cool down to room temperature. Through changing the heating time to 4 and 7 h, a series of samples were obtained and named as 31%-Ni-MOF-74/Ni_3N and Ni_3N, respectively.

Materials Characterization. Powder X-ray powder diffraction (PXRD) patterns were taken on a Rigaku SmartLab 9KW X-ray powder diffractometer with a Cu Kα radiation source (λ = 0.154178 nm). All diffraction data were obtained at a scan rate of 6 °/min^{-1} in the 2θ range from 5° to 80°. The crystal structure of Ni-MOF-74/Ni_3N was refined from PXRD data by using Rietveld method with Fullprof software. Result showed a fine fitness with the experiment data, where low convergence residuals were achieved with a final R_{wp} of 7.76%. Transmission electron microscopy (TEM) observations and energy dispersive spectroscopy (EDS) data were performed by using a JEM 2100F transmission electron microscope equipped with an EDX spectrometer at an accelerating voltage of 200 kV. X-ray photoelectron spectroscopy (XPS) was gained after measurement using an ESCALAB 250Xi spectrophotometer.

Electrochemical Characterizations. All electrochemical test of this subject was carried out on the CHI 760 electrochemical workstation. The electrochemical test was conducted under the three-electrode system and the prepared sample with a loading of 0.45 mg cm^{-2} (loaded Ni foam 0.4 × 0.5 cm^2) was then used as the working electrode. Simultaneously, the carbon rod and Hg/HgO electrode serve as the counter and reference electrodes, respectively.

In the linear sweep voltammetry (LSV) test, an argon saturated atmosphere needs to be formed. And the sweeping speed was set to 1 mV s^{-1} in Ar saturated atmosphere. In 1.0 M KOH (pH = 14), the test was performed in the potential range from -0.9 to -1.3 V, with Hg/HgO selected as the reference electrode. As for OER, Hg/HgO was chosen as the reference electrode, and test was performed in the potential range from 1.2 to 1.8 V. The potential was calibrated to the reversible hydrogen electrode (RHE) according to the following formula: E (vs RHE) = E (vs Hg/HgO) + 0.059 × pH + 0.098 or E (vs RHE) = E (vs SCE) + 0.059 × pH + 0.242. The precise value of the potential versus reversible hydrogen electrode (RHE) of the Hg/HgO electrode was calibrated through using 20 wt% Pt/C deposited onto the glassy carbon (GC) rotating disk electrode so that the hydrogen oxidation polarization curve at 5 mV s^{-1} can be obtained under hydrogen atmosphere. The electrochemically active surface areas (ECSA) have been inquired by the double-layer capacitance (C_{dl}) via CV. Specifically, Cyclic voltammetry (CV) curves of the electrocatalyst were measured in 1.0 mol L^{-1} KOH solution at scanning rates of 10, 20, 30, 40 and 50 mV s^{-1} in the non-Faraday interval, and C_{dl} was obtained by linear fitting. The electrochemical impedance spectroscopy (EIS) curves were recorded by maintaining an invariable potential in frequency from 0.01 to 100000 Hz in 1.0 M KOH solution.

Density Functional Theory (DFT) Calculation. The DFT calculations were carried out with generalized gradient approximation (GGA) and Perdew-Burke-Ernzerhof (PBE) functional for exchange correlation energy and ultrasoft pseudo-potentials to represent core-valance interaction on CASTEP code of the Materials Studio package of Accelrys Inc. The cutoff energy of 430 eV was settled and the self-consistent field (SCF) tolerance was $2×10^{-6}$ eV. The Ni_3N surface was selected with repetition in 3×3×2 unit and a vacuum width of 15 Å to ensure all atoms were thoroughly relaxed. The Monkhorst-Pack mesh k-points were sampled as 4×4×1 for surface calculation. And all energy difference of all planes does not exceed 0.01 eV. The hydrogen adsorption free energy $\triangle G_{*H} = E_{(M-H)} - E_{(M)} - 1/2E_{(H2)} + \triangle E_{(ZPE)} - T\triangle S$ ($\triangle E_{(ZPE)}$ and $\triangle S$ are the zero-point energy and entropy). Further, the water adsorption free energy $\Delta G_{H2O} = E_{(M-H2O)} - E_{(M)} - E_{(H2O)} + \Delta E_{(ZPE)} - T\Delta S$.

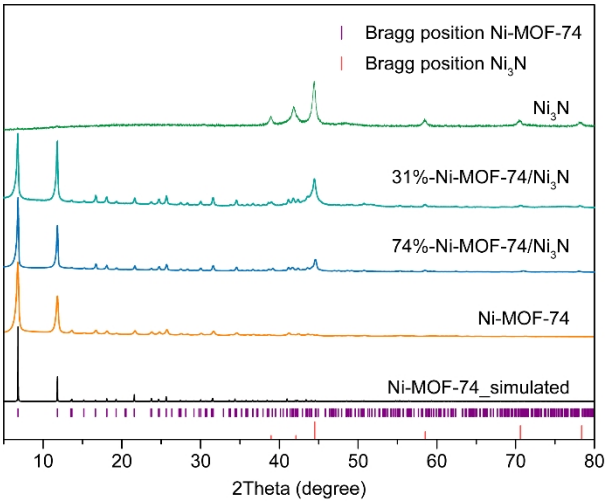

Figure S1. PXRD patterns of Ni-MOF-74/Ni_3N with different two-phase ratios.

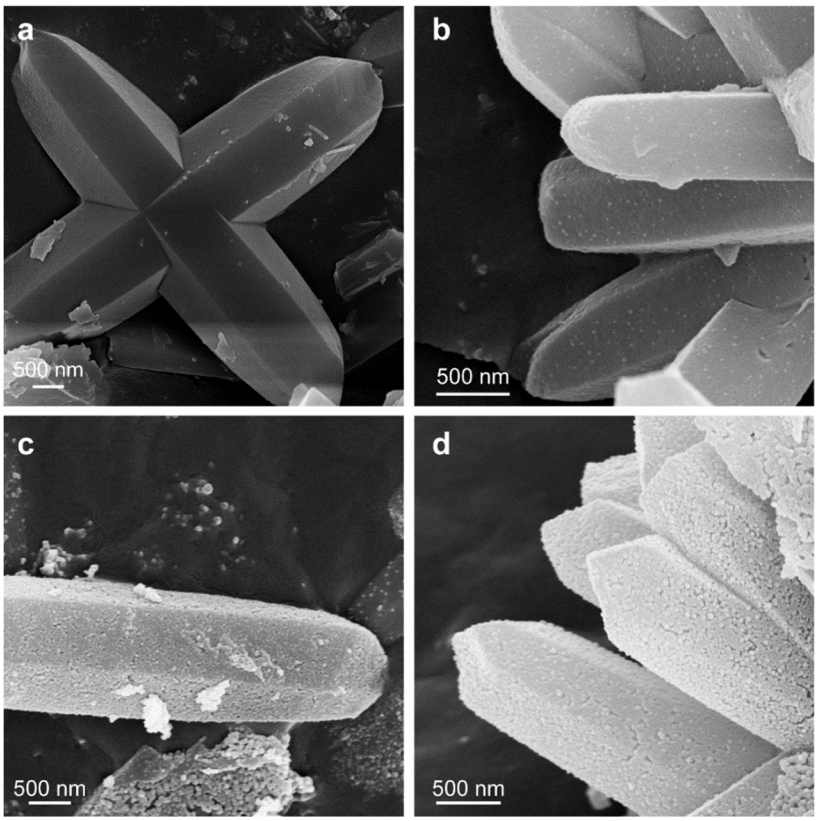

Figure S2. SEM images of Ni-MOF-74, 74%-Ni-MOF-74/Ni_3N, 31%-Ni-MOF-74/Ni_3N and Ni_3N.

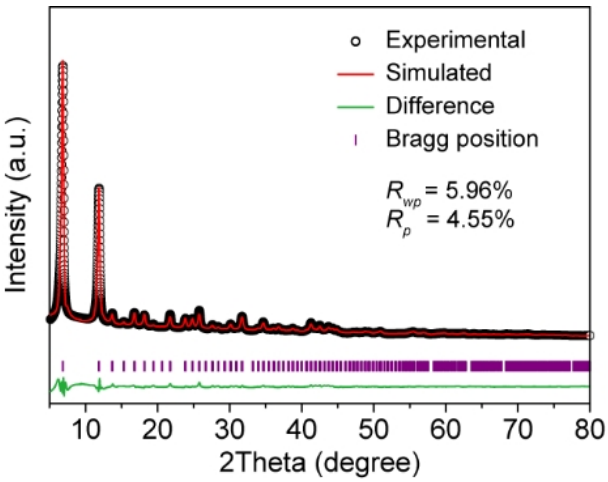

Figure S3. Retiveld refinement for Ni-MOF-74.

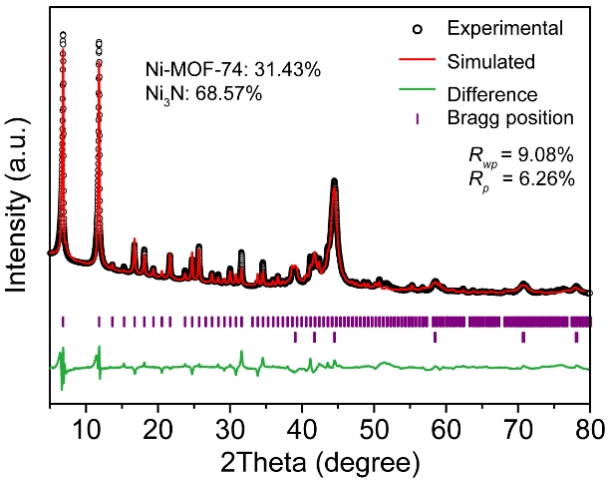

Figure S4. Retiveld refinement for 31%-Ni-MOF-74/Ni_3N.

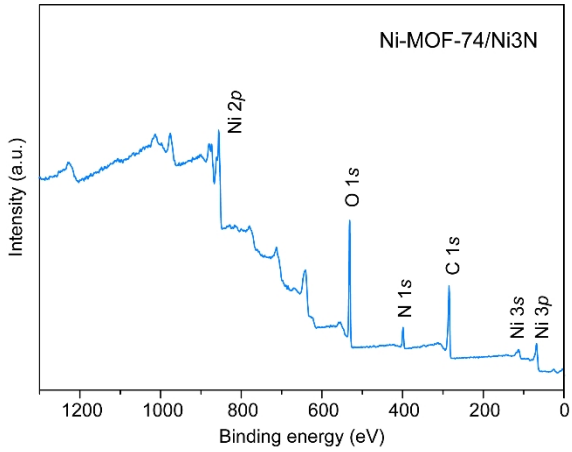

Figure S5. The survey scan XPS spectra of Ni-MOF-74/Ni_3N.

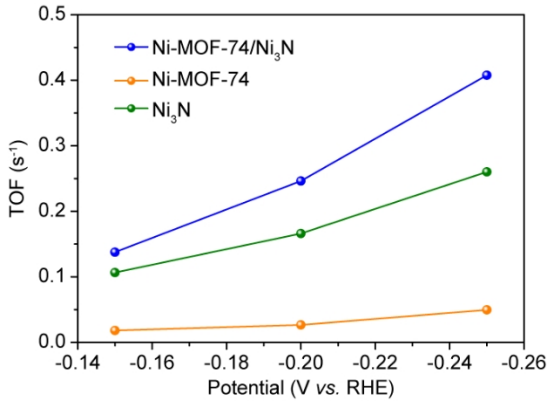

Figure S6. The TOF values of Ni-MOF-74/Ni_3N, Ni_3N and Ni-MOF-74.

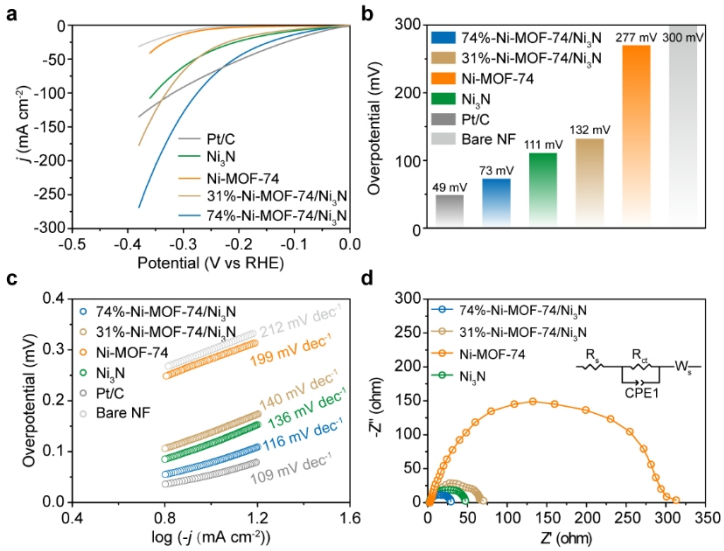

Figure S7. HER electrochemical performance of Ni-MOF-74/Ni_3N with different two-phase ratios and blank control. a) Polarization curves in 1.0 M KOH; (b) Comparison of overpotentials at 10 mA cm^{-2}; (c) Tafel plots of different catalysts; (d) Nyquist plots.

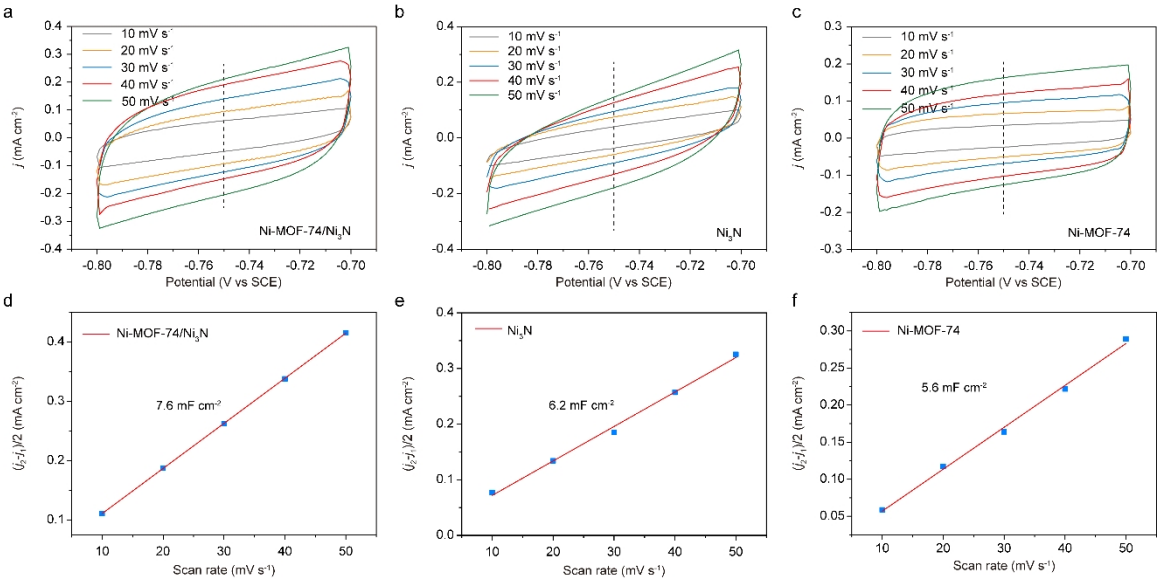

Figure S8. (a-c) CV curves and (d-f) C_{dl} of Ni-MOF-74/Ni_3N, Ni-MOF-74 and Ni_3N.

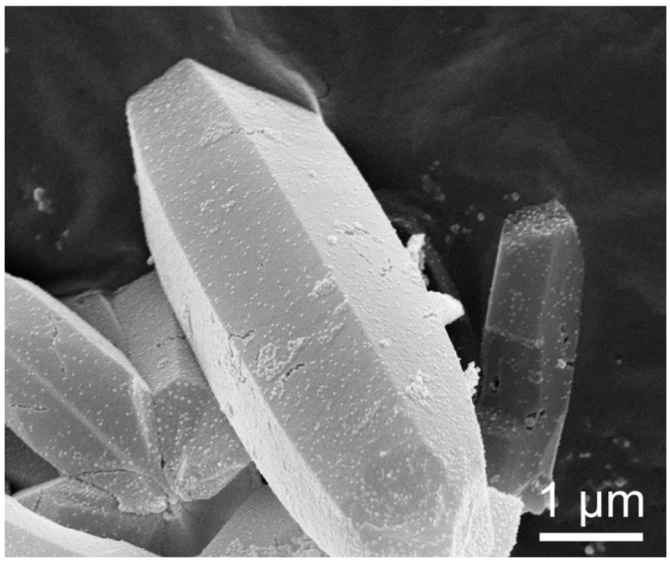

Figure S9. SEM image of Ni-MOF-74/Ni_3N after HER test in 1.0 M KOH solution.

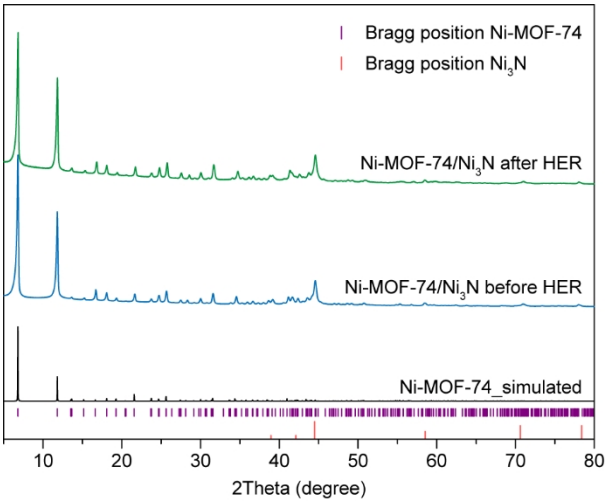

Figure S10. PXRD patterns of Ni-MOF-74/Ni_3N after HER test in 1.0 M KOH solution.

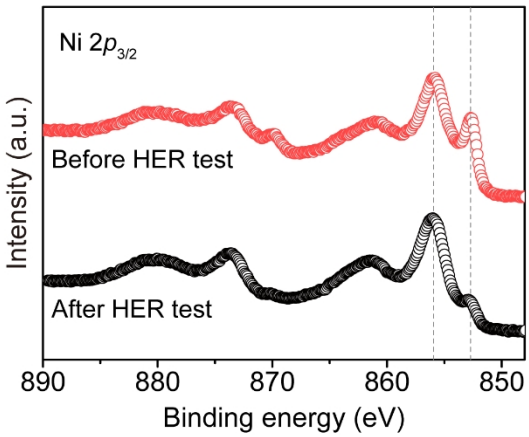

Figure S11. High resolution XPS spectra of Ni-MOF-74/Ni_3N before and after HER test in 1.0 M KOH solution.

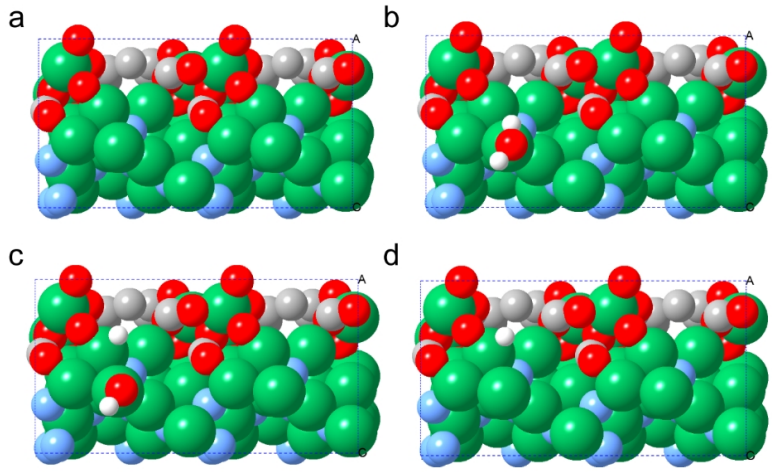

Figure S12. The most stable geometric configuration of adsorption structure on Ni-MOF-74/Ni_3N surface with top view (a) Ni-MOF-74/Ni_3N; (b) *H2O; (c) *H+*OH and (d) *H.

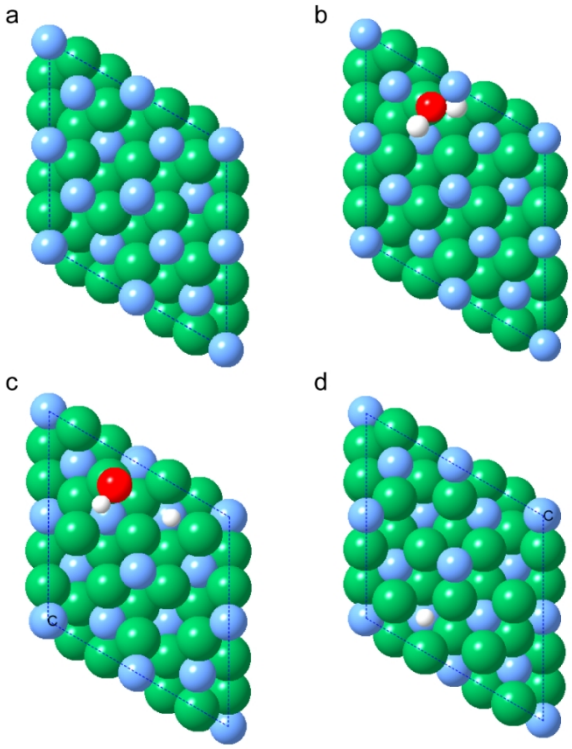

Figure S13. The most stable geometric configuration of adsorption structure on Ni_3N surface with top view (a) Ni_3N; (b) *H2O; (c) *H+*OH and (d) *H.

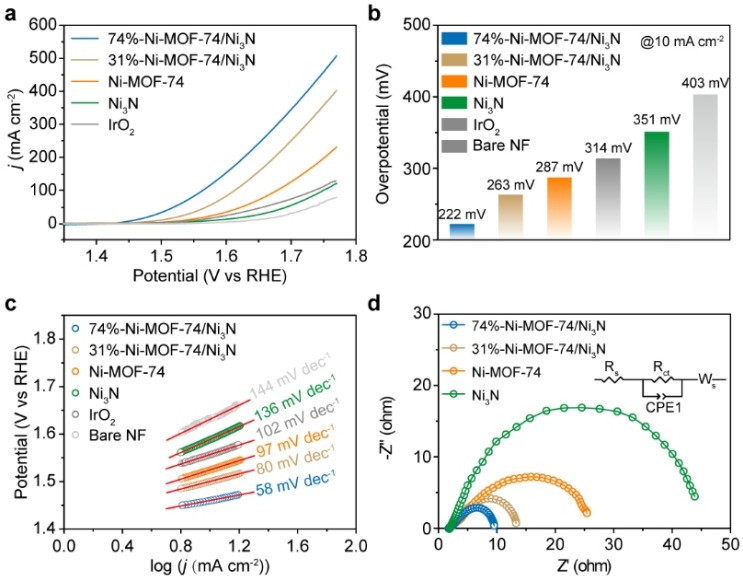

Figure S14. OER electrochemical performance of Ni-MOF-74/Ni_3N with different two-phase ratios and blank control. (a) Polarization curves in 1.0 M KOH; (b) Comparison of overpotentials at 10 mA cm^{-2}; (c) Tafel plots of different catalysts; (d) Nyquist plots.

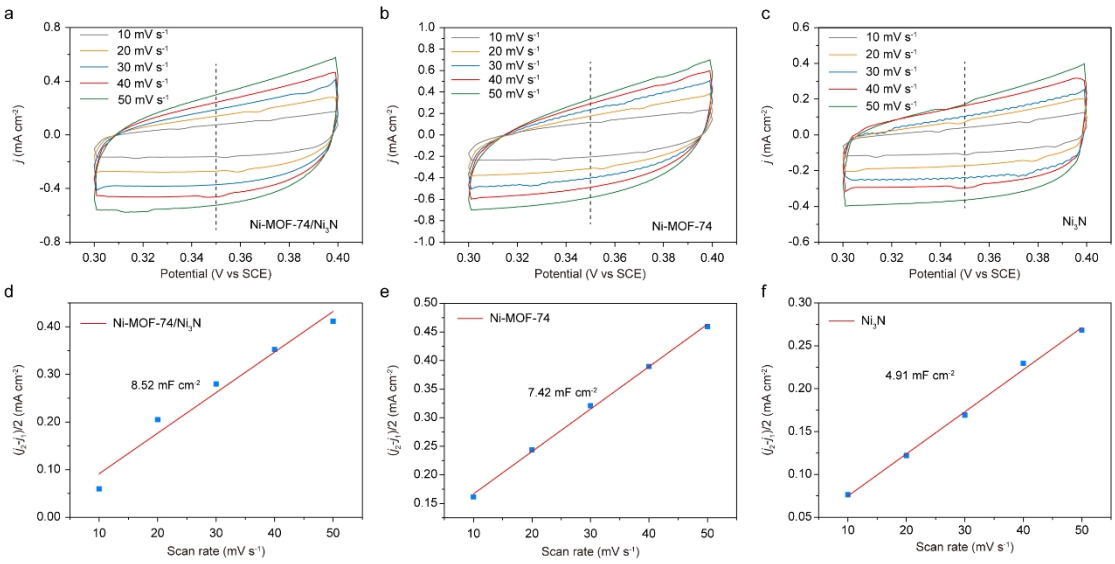

Figure S15. (a-c) CV curves and (d-f) C_{dl} of Ni-MOF-74/Ni_3N, Ni-MOF-74 and Ni_3N.

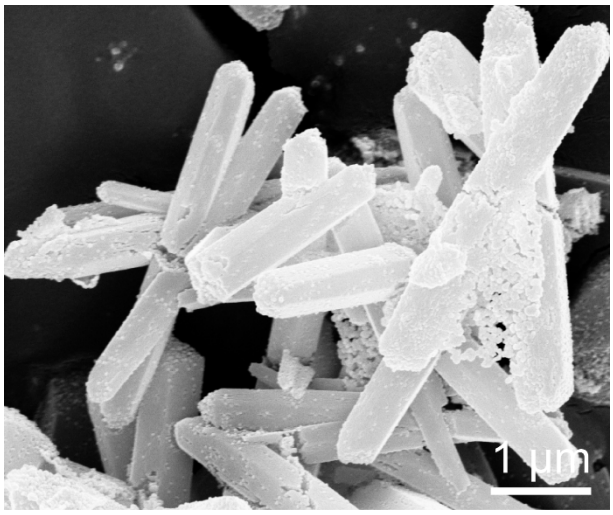

Figure S16. SEM image of Ni-MOF-74/Ni_3N after OER test in 1.0 M KOH solution.

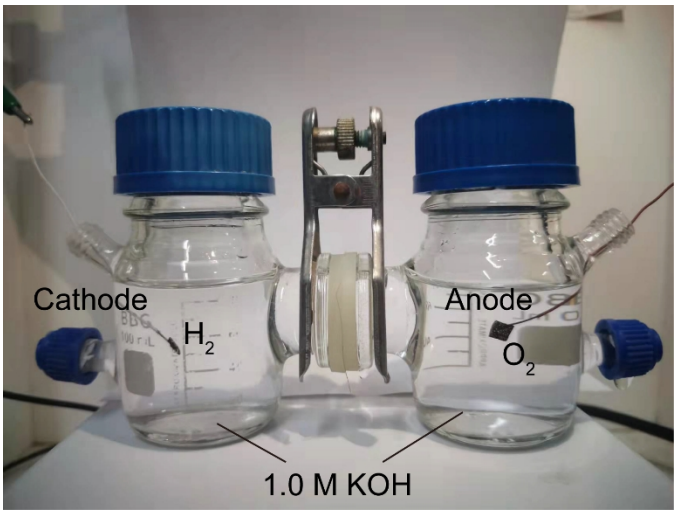

Figure S17. The evolution of hydrogen and oxygen gas bubbles for overall water splitting.

Table S1. Comparison of Representative MOF-based OER Catalysts in 1.0 M KOH Electrolyte

Catalyst	j (mA cm^{-2})	η (mV)	Reference
Ni-MOF-74/Ni_3N	**10**	**73**	**This work**
CoP/Co-MOF	10	34	1
NFN-MOF	10	87	2
NENU-500	10	237	3
NiFe-MOF	10	134	4
NCMC	10	169.5	5
Ni@CoO@CoNC	10	190	6
porous Ni_2P	10	168	7
Co@N-CNT	10	74	8
$Ni_{1.4}Co_{0.6}P$/NCNHMs	10	64.4	9
Ni_2P/rGO	10	142	10

Table S2. HER Electrochemical Rerformance

Electrocatalyst	R_s (Ω)	R_{ct} (Ω)
74%-Ni-MOF-74/Ni_3N	2.38	**27.12**
31%-Ni-MOF-74/Ni_3N	2.01	45.37
Ni_3N	2.28	64.93
Ni-MOF-74	3.49	311.07

Table S3. Comparison of Representative MOF-based OER Catalysts in 1.0 M KOH Electrolyte.

Catalyst	j (mA cm^{-2})	η (mV)	Reference
Ni-MOF-74/Ni_3N	**10**	**222**	**This work**
NiFe-MOF	10	240	4
Ni@CoO@CoNC	10	309	6
porous Ni_2P	10	320	7
Ni(Fe)-MOF	10	227	11
NCNTFs	10	370	12
N-NiFe-MOF	100	258	13
NiCo/Fe_3O_4-O-MOF-74	50	263	14
MIL-53(FeNi)/NF	100	252	15
CTGU-10c2	10	240	16
NNU-23	10	365	17
$(Ni_2Co_1)_{0.925}Fe_{0.075}$-MOF-NF	10	257	18
$A_{2.7}$B-MOF-$FeCo_{1.6}$	10	288	19
Ni-ZIF/Ni-B@NF	100	310	20
Ultrathin NiFe-MOF array	100	300	21
Miss-linker-Co-BDC	100	251	22

Table S4. OER Electrochemical Performance

Electrocatalyst	R_s (Ω)	R_{ct} (Ω)
74%-Ni-MOF-74/Ni_3N	2.49	**7.53**
31%-Ni-MOF-74/Ni_3N	3.98	11.83
Ni-MOF-74	2.69	26.89
Ni_3N	2.04	39.87

Table S5. Comparison of Representative Representative Transition Metal-based OER Catalysts in 1.0 M KOH Electrolyte.

Catalyst	j (mA cm^{-2})	E (V)	Reference
Ni-MOF-74/Ni_3N	**10**	**1.52**	**This work**
NFN-MOF/NF	10	1.56	2
NiFe-MOF	10	1.55	4
NCMC	10	1.63	5
Co@N-CNT	30	1.58	8
$Ni_{1.4}Co_{0.6}P$/NCNHMs	10	1.55	9
Ni_2P/rGO	10	1.61	10
Ni(Fe)-MOF	10	1.537	11

n REFERENCES

(1) T. Liu, P. Li, N. Yao, G. Cheng, S. Chen, W. Luo, Y. Yin, *Angew. Chem.* **2019**, 131, 4727-4732.
(2) D. Senthil Raja, X.-F. Chuah, S.-Y. Lu, *Adv. Energy Mater.* **2018**, 8, 1801065.
(3) J.-S. Qin, D.-Y. Du, W. Guan, X.-J. Bo, Y.-F. Li, L.-P. Guo, Z.-M. Su, Y.-Y. Wang, Y.-Q. Lan, H.-C. Zhou, *J. Am. Chem. Soc.* **2015**, 137, 7169-7177.
(4) J. Duan, S. Chen, C. Zhao, *Nat. Commun.* **2017**, 8, 15341.
(5) X. Wei, Y. Zhang, H. He, D. Gao, J. Hu, H. Peng, L. Peng, S. Xiao, P. Xiao, *Chem. Commun.* **2019**, 55, 6515-6518.
(6) G. Cai, W. Zhang, L. J, S.-H. Yu, H.-L. Jiang, *Chem.* **2017**, 2, 791-802.
(7) Q. Wang, Z. Liu, H. Zhao, H. Huang, H. Jiao, Y. Du, *J. Mater. Chem. A* **2018**, 6, 18720-18727.
(8) L. Yang, H. Li, Y. Yu, Y. Wu, L. Zhang, *Appl. Catal. Environ.* **2020**, 271, 118939.
(9) S. Fan, J. Zhang, Q. Wu, S. Huang, J. Zheng, D. Kong, S. Chen, Y. Wang, L. K. Ang, Y. Shi, H.Y. Yang, *J. Phys. Chem. Lett.* **2020**, 11, 3911-3919.
(10) L. Yan, H. Jiang, Y. Xing, Y. Wang, D. Liu, X. Gu, P. Dai, L. Li, X. Zhao, *J. Mater. Chem. A* **2018**, 6, 1682-1691.
(11) C. Cao, D.-D. Ma, Q. Xu, X.-T. Wu, Q.-L. Zhu, *Adv. Funct. Mater.* **2019**, 29, 1807418.
(12) B.Y. Xia, Y. Yan, N. Li, H.B. Wu, X.W.D. Lou, X, Wang, *Nat. Energy* **2016**, 1, 15006.
(13) N. Yao, H. Jia, Z. Fan, L. Bai, W. Xie, H. Cong, S. Chen, W. Luo, *J. Energy Chem.* **2022,** 64, 531-537.
(14) F.-L. Li, Q. Shao, X. Huang, J.-P. Lang, *Angew. Chem. Int. Ed.* **2018**, 57, 1888-1892.
(15) X. Wang, H. Xiao, A. Li, Z. Li, S. Liu, Q. Zhang, G. Yun, L. Zheng, C. Chen, D. Wang, D. Peng, L. Gu, X. Han, J. Li, Y. Li, *J. Am. Chem. Soc.* **2018**, 140, 15336-15341.
(16) F. Sun, G. Wang, Y. Ding, C. Wang, B. Yuan, Y. Lin, *Adv. Energy Mater.* **2018**, 8 1800584.
(17) W. Zhou, D.-D. Huang, Y.-P. Wu, J. Zhao, T. Wu, J. Zhang, D.-S. Li, C. Sun, P. Feng, X. Bu, *Angew. Chem. Int. Ed.* **2019**, 58, 4227-4231.
(18) X. L. Wang, L.-Z. Dong, M. Qiao, Y.-G. Tang, J. Liu, Y. Li, Y. Lan, S. L. Li, J. X. Su, Y.-Q. Lan, *Angew. Chem. Int. Ed.* **2018**, 57, 9660-9664.
(19) Q. Qian, Y. Li, Y. Liu, L.Yu, G. Zhang, *Adv. Mater.* **2019**, 31, 1901139.
(20) D. S. Raja, X. Chuah, S.-Y. Lu, *Adv. Energy Mater.* **2018**, 8, 1801065.
(21) H. Xu, B. Fei, G. Cai, Y. Ha, J. Liu, H. Jia, J. Zhang, M. Liu, R. Wu, *Adv. Energy Mater.* **2020**, 10, 1902714.
(22) J. Duan, S. Chen, C. Zhao, *Nat. Commun.* **2017**, 8, 15341-15341.